Colloid Polym Sci 280: 254–259 (2002)

ORIGINAL CONTRIBUTION

Norbert Stribeck

Utilising spatial frequency filtering to extract nanoscale layer structure information from isotropic small-angle X-ray scattering data

Received: 24 July 2001
Accepted: 12 September 2001

N. Stribeck
Universität Hamburg, Institut für Technische und Makromolekulare Chemie, 20146 Hamburg, Germany
e-mail: norbert.stribeck@desy.de
Tel.: +49-40-428383615
Fax: +49-40-428386008

Abstract A separation method by spatial frequency filtering of the diffuse background of small-angle X-ray scattering (SAXS) is transferred to the case of isotropically scattering samples of polymer materials. Analysis of the residual discrete SAXS is demonstrated. Evaluations of model scattering curves from lamellar two-phase systems show that this technique, in general, results in a good separation. If samples with pure particle scattering or such with rough domain surfaces are investigated, the separation of a suitable background is possible, but is prone to some uncertainty which is estimated. In the case of particle scattering from lamellae the problem is solved by fitting a model function considering polydispersity to the Lorentz-corrected scattering intensity. After background correction the residual information on the distorted nanostructure is collected in an interface distribution function, from which topological parameters can be recovered with high accuracy. These parameters comprise average layer thicknesses and parameters of particle polydispersity. Parameter recovery is achieved by nonlinear regression with model functions describing stacking statistics. Automated versions of the technique are suited to process and analyse series of polymers collected in time-resolved synchrotron radiation experiments.

Keywords Small-angle scattering · Background separation method · Low-pass filter · Polydispersity · Time-resolved

Introduction

Polymer nanostructures are found in almost any isotropic polymer material. They exhibit poor long-range order, in general. Thus, the corresponding discrete small-angle X-ray scattering (SAXS) comprises a few broad peaks and is superposed by a strong diffuse background which should be subtracted before quantitative analysis is undertaken. Such analysis is only reasonable if it is based on a topological model, the validity of which has been verified by other methods. Images from electron microscopy [1, 2] resulted in the cognition that the simple model of a lamellar two-phase system can be applied to the nanostructure of many polymer materials. Owing to this promising starting position, researchers have been concentrating on the solution of the SAXS analysis problem for a long time.

The basic properties of scattering from a multiphase system have been discussed by Porod [3]. Debye's general correlation function [4] has paved the way to analysis of scattering data from distorted structures in the physical space. The practical applicability of this concept for the case of a lamellar two-phase system has been exhausted in the work of Vonk and coworkers [5–8]

on their one-dimensional correlation function. Utilising the concept of the correlation function, the considerable influence of polydispersity on scattering data can unfortunately only be taken into account in a rudimentary way. Thus, correlation function analysis, in virtually any practical case, assumes that layer thicknesses in the lamellar system vary little about an average value [9]. The consequences of this simplification are documented [10].

A solution to this dilemma has been devised by Méring and coworkers [11–15]. Their chord distribution function (CDF) is the second derivative of the correlation function and it is built from particle size distributions, which are basic to structural analysis. This concept was first made applicable for a wide range of practical problems by the interface distribution function (IDF), as deduced by Ruland and Stribeck [16–18].

In particular, when attempting to employ the IDF or the CDF for SAXS analysis, the importance of a meaningful background separation becomes palpable [10, 18–21]. In general, various contributions to the background are superimposed and are difficult to separate from each other and from the discrete SAXS. Considering the IDF, $g_1(x)$, the mentioned uncertainty leads to considerable inaccuracy in the vicinity of zero, where thin lamellae show up. Here the shape of the curve is affected by the chosen separation of several slowly varying backgrounds to the SAXS. Because of this importance to subsequent analysis, the background elimination procedure chosen should be described clearly.

More and more, the IDF method is used to interpret the nanostructure inherent to SAXS data [10, 20, 22–38]. Furthermore the volume of data to be analysed is bulging because of an increasing number of time-resolved experiments. Thus, there is good reason to define background subtraction in a manner restricting user intervention and allowing automated processing of series of data [20]. Here, a novel method of background subtraction for data from isotropic samples which meets the mentioned requirements is proposed. It is based on a technique which has recently been devised for background correction of anisotropic SAXS patterns with fibre symmetry [39].

Description of the method

The established technique

Let $I(s)$ be the observed isotropic SAXS intensity of a lamellar two-phase system measured with point focus. Modifications for the case of line focus, $\tilde{I}(s)$, are well known. The magnitude of the scattering vector is defined by $s = (2/\lambda)\sin\theta$, with λ the wavelength of radiation and 2θ the scattering angle. Then a one-dimensional intensity, $I_1(s) = 2\pi s^2 I(s)$, is obtained by "Lorentz correction". It describes the scattering arising from electron density changes in the direction normal to the surfaces of the lamellae. Because $I(s)$ describes a nonideal [19, 21, 25, 40–42] two-phase system, the one-dimensional Fourier back transformation,

$$-G_1(s) = \mathscr{F}^{-1}[g_1(x)] \ , \tag{1}$$

of the IDF to be studied, $g_1(x)$, is an interference function,

$$G_1(s) = [I(s) - I_{\mathrm{Fl}}(s) - I_{\mathrm{R}}(s)]\left[s^4/F(\sigma_i s)\right] - A_{\mathrm{P}} \ , \tag{2}$$

which carries several terms describing deviations from an ideal two-phase system. These are $I_{\mathrm{Fl}}(s)$, a background from short-range density fluctuations throughout the sample, $I_{\mathrm{R}}(s)$, a background from short-range roughness of the domain surfaces, and $F(\sigma_i s)$, a deviation of Porod's law (s^4), caused from a finite phase transition zone at the domain interfaces. A_{P} governs the asymptotic behaviour of the scattering intensity according to Porod's law.

Where $I_{\mathrm{Fl}}(s)$ and $I_{\mathrm{R}}(s)$ are concerned, the only assured prediction says that mainly the even, low-order coefficients of their Taylor expansion series differ from zero. Thus, these backgrounds are slowly varying functions in s. Although $F(\sigma_i s)$ can be defined more precisely, its effect on the scattering curve varies slowly as well. If the different effects of non-ideal structure are studied separately after modelling the background by a Taylor polynomial, consistent results are achieved in rare cases only [5, 43]. However, after further restriction to constant fluctuation and roughness backgrounds, more data sets could be investigated successfully [8, 10, 21].

The proposed technique

In a first step to background subtraction let us define an estimated constant background, c_{Fl}, by minimising the function

$$T_{\mathrm{c}}\left(c_{\mathrm{Fl}}; A_{\mathrm{p}}\right) = \sum_k \left[s_k^4 (I_k - c_{\mathrm{Fl}}) - A_{\mathrm{P}}\right]^2 \ , \tag{3}$$

with the sum being extended over all measured points in the region where Porod's law is estimated to be valid. Then,

$$I_{\mathrm{Pl}}(s) = s^4 [I(s) - c_{\mathrm{Fl}}] \tag{4}$$

is computed, which ends in an almost horizontal asymptote, if Porod's region is chosen reasonably. Now let us define a low-pass filter operator, $f_{\mathrm{l},x_{\mathrm{c}}}()$, with a cutoff frequency, x_{c}, defined in real space. A first-order Butterworth filter,

$$f_{\mathrm{l},x_{\mathrm{c}}}[I_{\mathrm{Pl}}(s)] = \mathscr{F}^{-1}\left(\mathscr{F}[I_{\mathrm{Pl}}(s)](x)\frac{1}{(1 + x/x_{\mathrm{c}})^2}\right) \ , \tag{5}$$

has proved feasible in many fields of research. The method for two different scattering curves using a standard cutoff frequency $x_{\mathrm{c}} = 0.1/s_{\max}$ is demonstrated in Figs. 1 and 2. $s_{\max}$ is the upper limit of the estimated Porod region. In a second step to background correction now the low-pass filtered background is subtracted and

$$G_1(s) = I_{\mathrm{Pl}}(s) - f_{\mathrm{l},x_{\mathrm{c}}}[I_{\mathrm{Pl}}(s)], \tag{6}$$

the interference function, is obtained. Additionally, in order to minimise artifacts in the Fourier transformed results from the next step, the curves are multiplied by a "Hann" function, well known in the field of digital image processing [44]. Similar functions are addressed as "cosine-bell", "Hanning" or "Hamming" window.

First, it is pointed out that the effective background correction function is not a constant anymore. The combination of the two background correction steps results in a slowly varying background function in s, as is requested from theoretical consideration. Although this method appears to be more adapted than the subtraction of a constant background, it cannot be guaranteed that the proposed choice is the correct one. So there is, in fact, no relief where the correct determination of small-sized domains is concerned. We cannot estimate the validity of the background correction; therefore, evidence concerning smaller size parameters from SAXS data remains limited.

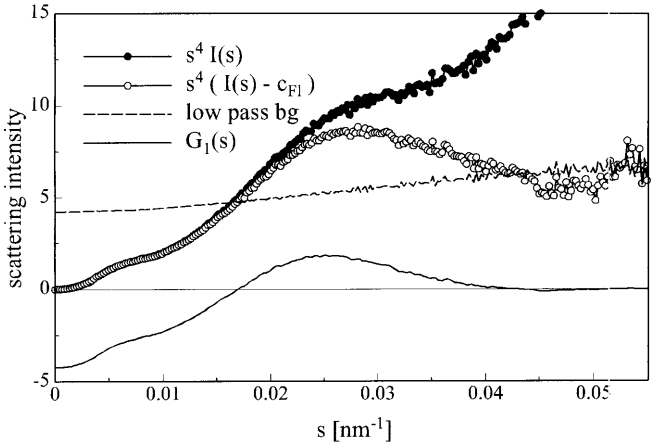

Fig. 1 From scattering intensity to interference function by low-pass filtering. Ultrahigh-molecular-weight polyethylene sample which does not allow separation of different background components

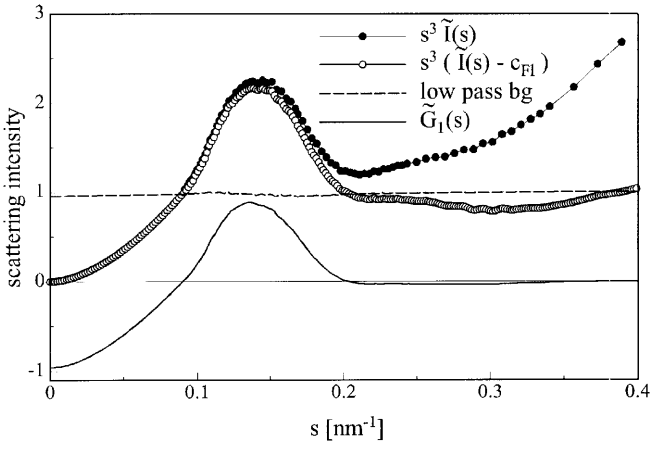

Fig. 2 From scattering intensity to interference function by low-pass filtering of a slit-smeared, $\tilde{I}(s)$, scattering curve. Polyethylene sample which allows separation of fluctuation and interfacial width in the background

Second, it should be mentioned that in the case of considerable domain surface roughness, i.e. whenever the integral $\int G_1(s)\mathrm{d}s$ becomes strongly negative, the background elimination may be carried out repeatedly, until the postulation $\int G_1(s)\mathrm{d}s \approx 0$ is fulfilled. If such iterated interference functions are analysed, it should be checked carefully if the substantial aspects of the two-phase structure have passed the applied cascade of spatial frequency filters. Most probably such an iteration will erase information on small and distorted domains.

Tests of the method

Comparison with manual background subtraction

After $G_1(s)$ is determined, the inverse of Eq. (1) demonstrates how to compute the interface distribution $g_1(x)$. Two results for the scattering curve from Fig. 2 are shown in Fig. 3. The dashed curve was obtained manually after determining the values of a constant fluctuation background and a finite phase transition zone. The solid line was computed automatically after a single spatial frequency filtering step. It is observed that because of the increased flexibility of the low-pass filtered background the solid line IDF starts with a somewhat narrower positive peak. This makes the residual nanostructure appear to be somewhat more perfect.

In order to quantify nanostructural data, both curves were fitted by the model of a one-dimensional stacking statistics of layers [42, 45]. The results are presented in Table 1 and show agreement within the range of the computed intervals of confidence.

Evaluation of layer stack model scattering curves

The last section demonstrated the relative compatibility between the established method of background subtraction and the spatial frequency filtering technique. Here the absolute accuracy of the new method is demonstrated. For this purpose model scattering curves, $I(s)$, of layer stacks were computed utilising well-known equations [35], 5% relative statistical noise was applied and, finally, the interface distribution function, $g_1(x)$, was

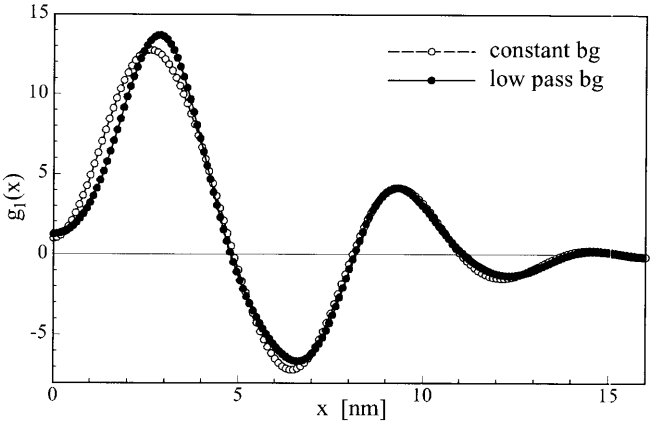

Fig. 3 Two interface distribution functions, $g_1(x)$, determined from one sample after different kinds of background subtraction

Table 1 Comparison of layer stack nanostructure parameters determined after different kinds of background subtraction. Mean crystalline and amorphous thicknesses, $\bar{t}_c$ and $\bar{t}_a$. Relative width parameters of layer thickness distributions, $\sigma_c/\bar{t}_c$ and $\sigma_a/\bar{t}_a$, respectively

	Constant background	Low-pass background
$\bar{t}_c$ (nm)	3.9 ± 0.2	4.3 ± 0.4
$\bar{t}_a$(nm)	2.8 ± 0.1	2.4 ± 0.4
$\sigma_c/\bar{t}_c$	0.35 ± 0.05	0.29 ± 0.03
$\sigma_a/\bar{t}_a$	0.39 ± 0.03	0.44 ± 0.03

determined utilising the spatial filtering algorithm. A typical result is presented in Table 2. The results show that only the smaller of the two layer thicknesses (here $\bar{t}_a$) is somewhat overestimated. The other structural parameters are very close to the parameters predefined in the model.

The intervals of confidence are computed by the nonlinear regression algorithm [45, 46]. The small but significant deviations between model and evaluation exhibit the effect of background overcorrection. Similar model evaluations can be performed on a routine basis using actual models, structural parameters, backgrounds and noise whenever the introduction of methodical error into structural parameter determination is estimated.

The extreme limit: layer particle scattering

Scattering and analysis of layer stacks have been treated. Now the case of an ensemble of uncorrelated lamellae is considered; this does not show interference effects. It is demonstrated that the method is even suitable to yield estimated values for the average layer thickness, $\bar{t}_c$, and the polydispersity, represented by $\sigma_c/\bar{t}_c$, although in this case a fit of a suitable model function on the Lorentz-corrected scattering curve yields more accurate parameters. The limit to be discussed is observed just below the melting temperature during melting or crystallisation of a polymer. Owing to missing interference it is expected that background subtraction by spatial frequency is most uncertain in this case.

The importance of domain polydispersity in the field of the nanostructure of polymer materials has been evidenced by numerous SAXS investigations and by electron microscopy [47, 48]. It is thus a coarse approximation to describe the isotropic scattering of an ensemble of uncorrelated lamellae by the particle scattering of the average layer, $\bar{t}_c$, [3, 49] only:

$$I(s) = 2A_P \frac{\sin^2(\pi \bar{t}_c s)}{s^4} \quad . \tag{7}$$

In some works even more extensive approximations have been applied which aim at linearisation of the scattering data [49, 50] in order to simplify determination of the layer thickness from the scattering data.

In order to consider polydispersity with ensembles of polymer nanoscale particles, Porod [51] extended a graphical method proposed by Hosemann, but these days computer-based evaluation methods [42, 45, 52, 53], which are more powerful and less restrictive, should be preferred. If the shape of the layer thickness distributions is modelled by a Gaussian or related functions [42], computing time is no problem. More suitable base functions are known [54, 55], but still require unendurable computing effort. It is easily deduced [45] that for the assumption of Gaussian layer thickness distributions Eq. (7) can be extended to yield

$$2\pi s^2 I(s) = I_1(s) = \frac{W}{s^2}[1 - H_c(s)], \tag{8}$$

with

$$H_c(s) = \cos(2\pi \bar{t}_c s) \exp\left(-2\pi^2 \sigma_c^2 s^2\right).$$

The function $H(s)$ is the Fourier transform of the normalised layer thickness distribution, $h_c(x)$, and the quantity $W = 2\pi A_P$ its weight. An ensemble of uncorrelated lamellae is completely characterised by these parameters. From Eq. (8) it is concluded that the "interference function" $s^2 I_1(s)$ contains the "reciprocal" layer thickness distribution in undistorted shape and thus is, in principal, the most appropriate starting point for its analysis. Cser's argument [56] criticising the use of even the milder Lorentz correction is thus not only based on obsolete and awkward approximations, but is also vitiated by mathematical deduction.

For fitting transformed SAXS data, adapted model functions can easily be derived from Eq. (8). Several experimental and model data sets were tested and it was confirmed that fits of $I_1(s)$ and $s^2 I_1(s)$ result in accurate values for structural parameters, whereas the fit on $I(s)$ ends in considerable uncertainty. The results are reported in Table 3.

Although the results of fitting $s^4 I(s)$ are accurate, it should be considered that background correction for such data is much more critical than for a Lorentz-corrected curve. Parameters directly determined from the measured intensity are inaccurate. Computed estimated intervals of confidence from nonlinear regression clearly indicate the problem.

In the last column values are listed which were obtained after background correction utilising the low-pass filter, computing the degenerate IDF and analysing the resulting layer thickness distribution. It is obvious that a considerable fraction of thin lamellae from the model were attributed to the background, resulting in an underestimation of domain polydispersity and an overestimation of the average layer thickness.

Table 2 Test of the spatial frequency filtering method by means of a model scattering curve (one-dimensional stacking statistics). Mean crystalline and amorphous thicknesses, $\bar{t}_c$ and $\bar{t}_a$. Relative width parameters of layer thickness distributions, $\sigma_c/\bar{t}_c$ and $\sigma_a/\bar{t}_a$, respectively

	Model parameters	Evaluated parameters
$\bar{t}_c$(nm)	80	80.5 ± 0.1
$\bar{t}_a$(nm)	40	41.7 ± 0.1
$\sigma_c/\bar{t}_c$	0.2	0.206 ± 0.001
$\sigma_a/\bar{t}_a$	0.4	0.391 ± 0.004

Table 3 Comparison of methods for the determination of structural parameters of lamellar two-phase systems in the limiting case of uncorrelated lamellae. Estimate of quality by evaluation of a noisy (5% relative noise) model scattering curve based on point-focus scattering intensity, $I(s)$, Lorentz-corrected intensity, $s^2I(s)$, interference function, $s^4I(s)$, and by evaluation of the degenerate interface distribution function, $g_1(x)$

Background correction	Model No	$I(s)$ No	$s^2I(s)$ No	$s^4I(s)$ No	$g_1(x)$ Yes
W	1	0.82 ± 0.13	0.99 ± 0.01	0.99 ± 0.01	0.94 ± 0.07
$\bar{t}_c$	70	85 ± 11	71 ± 1	71 ± 1	80 ± 1
$\sigma_c/\bar{t}_c$	0.5	0.25 ± 0.15	0.48 ± 0.02	0.48 ± 0.02	0.42 ± 0.01

Conclusion

The method of SAXS background subtraction by low-pass filtering allows one to evaluate series of scattering curves automatically. The remaining curve contains a substantial fraction of topological information on the system. Some inaccuracy with the determination of small layer thicknesses related to any background determination has been demonstrated in different ways. Despite certain restrictions for the analysis of uncorrelated particles, this method appears well suited to investigate variations of nanostructure of polymer materials on strain or temperature by time-resolved SAXS. Thus, it is expected to become a valuable tool to elucidate structure-forming processes as well as the relation between structure and properties of polymer materials.

References

1. Claver GC Jr, Buchdahl R, Miller RL (1956) J Polym Sci 20:202–205
2. Kanig G (1977) Colloid Polym Sci 255:1005–1007
3. Porod G (1951) Kolloid-Z 124:83–114
4. Debye P, Anderson HR Jr, Brumberger H (1957) J Appl Phys 28:679–683
5. Vonk CG (1973) J Appl Crystallogr 6:81–86
6. Vonk CG, Kortleve G (1697) Kolloid Z Z Polym 220:19–24
7. Kortleve G, Vonk CG (1968) Kolloid Z Z Polym 225:124–131
8. Vonk CG, Pijpers AP (1985) J Polym Sci Part B Polym Phys 23:2517–2537
9. Strobl GR, Schneider M (1980) J Polym Sci Part B Polym Phys 18:1343–1359
10. Santa Cruz C, Stribeck N, Zachmann HG, Baltà Calleja FJ (1991) Macromolecules 24:5980–5990
11. Méring J, Tchoubar D (1968) J Appl Crystallogr 1:153–165
12. Tchoubar D, Méring J (1969) J Appl Cryst 2:128–138
13. Méring J, Tchoubar D, Schiller C (1967) Bull Soc Fr Mineral Cristallogr 40:436–444
14. Méring J, Tchoubar-Vallat D (1965) CR Acad Sci Paris 261:3096–3099
15. Méring J, Tchoubar-Vallat D (1966) CR Acad Sci Paris 262:1703–1706
16. Ruland W (1977) Colloid Polym Sci 255:417–427
17. Ruland W (1978) Colloid Polym Sci 256:932–936
18. Stribeck N, Ruland W (1978) J Appl Crystallogr 11:535–539
19. Ruland W (1971) J Appl Crystallogr 4:71–73
20. Hsiao BS, Verma RK (1998) J Synchrotron Radiat 5:23–29
21. Stribeck N, Fakirov S, Sapoundjieva D (1999) Macromolecules 32:3368–3378
22. Fischer L, Haschberger R, Ziegeldorf A, Ruland W (1982) Colloid Polym Sci 260:174–181
23. Fiedel HW, Wenig W (1989) Colloid Polym Sci 267:369–398
24. Stribeck N, Zachmann HG, Bayer RK, Baltà Calleja FJ (1997) J Mater Sci 32:1639–1647
25. Wolff T, Burger C, Ruland W (1994) 27:3301–3309
26. Stribeck N, Sapoundjieva D, Denchev Z, Apostolov AA, Zachmann HG, Stamm M, Fakirov S (1997) Macromolecules 30:1329–1339
27. Schmidtke J, Strobl G, Thurn-Albrecht T (1977) Macromolecules, 30:5804–5821
28. Stribeck N, Reimers C, Ghioca P, Buzdugan E (1998) J Polym Sci Part B Polym Phys 36:1423–1432
29. Chen H-L, Li L-J, Lin T-L (1998) Macromolecules 31:2255–2264
30. Thünemann AF, Lochhaas KH (1998) Langmuir 14:6220–6225
31. Heck B, Hugel T, Iijima M, Strobl G (2000) Polymer 41:8839–8848
32. Stribeck N (2000) ACS Symp Ser 739:41–56
33. Thünemann AF, Ruland W (2000) Macromolecules 33:2626–2631
34. Iijima M, Strobl G (2000) Macromolecules 33:5204–5214
35. Wutz C, Stribeck N, Gieseler D (2000) Colloid Polym Sci 278:1061–1069
36. Heck B, Hugel T, Iijima M, Sadiku E, Strobl G (1999) New J Phys 1:17.1–17.29
37. Flores A, Pietkiewicz D, Stribeck N, Roslaniec Z, Baltà Calleja FJ (2001) Macromolecules 34:8094–8100
38. Fu Q, Heck B, Strobl G, Thomann Y (2001) Macromolecules 34:2502–2511
39. Stribeck N (2001) J Appl Crystallogr 34:496–503
40. Ruland W (1987) Macromolecules 20:87–93
41. Semenov A (1994) Macromolecules 27:2732–2735
42. Stribeck N (1993) Colloid Polym Sci 271:1007–1023
43. Siemann U, Ruland W (1982) Colloid Polym Sci 260:999–1010
44. Press WH, Teukolsky SA, Vetterling WT, Flannery BP (1992) Numerical recipes. Cambridge University Press, Cambridge
45. Stribeck N (1989) Colloid Polym Sci 267:301–310
46. Draper NR, Smith H (1980) Applied regression analysis, 2nd edn. Wiley, New York

47. Voigt-Martin IG, Stack GM, Peacock AJ, Mandelkern L (1987) J Polym Sci Part B Polym Phys 27:957–965
48. Voigt-Martin IG, Mandelkern L (1989) J Polym Sci Part B Polym Phys 27:967–991
49. Vonk CG (1988) Makromol Chem Makromol Symp 15:215–222
50. Kratky O, Laggner P (1987) Encycl Phys Sci Technol 14:693–742
51. Porod G (1961) Fortschr Hochpolym-Forsch 2:363–400
52. Reinhold C, Fischer EW, Peterlin A (1964) J Appl Phys 35:71–74
53. Glatter O (1980) J Appl Crystallogr 13:577–584
54. Stribeck N (1993) J Phys IV 3(C8):507–510
55. Marichev OI (1983) Handbook of integral transforms of higher transcendental functions. Ellis Horwood, Chichester
56. Cser F (2001) J Appl Polym Sci 80:358–366